

High contrast D₁ line electromagnetically induced transparency in nanometric-thin rubidium vapor cell

Armen Sargsyan¹, Claude Leroy², Yevgenya Pashayan-Leroy², Rafayel Mirzoyan¹, Aram Papoyan¹, David Sarkisyan¹

¹ Institute for Physical Research, NAS of Armenia, Ashtarak-2, 0203, Armenia

² Laboratoire Interdisciplinaire Carnot de Bourgogne, UMR CNRS 5209 - Université de Bourgogne, F-21078 Cedex, Dijon, France

The date of receipt and acceptance will be inserted by the editor

Abstract Electromagnetically induced transparency (EIT) on atomic D₁ line of rubidium is studied using a nanometric-thin cell with atomic vapor column length in the range of $L = 400 - 800$ nm. It is shown that the reduction of the cell thickness by 4 orders as compared with an ordinary cm-size cell still allows to form an EIT resonance for $L = \lambda$ ($\lambda = 794$ nm) with the contrast of up to 40 %. Remarkable distinctions of EIT formation in nanometric-thin and ordinary cells are demonstrated. Despite the Dicke effect of strong spectral narrowing and increase of the absorption for $L = \lambda/2$, EIT resonance is observed both in the absorption and the fluorescence spectra for relatively low intensity of the coupling laser. Well resolved splitting of the EIT resonance in moderate magnetic field for $L = \lambda$ can be used for magnetometry with nanometric spatial resolution. The presented theoretical model well describes the observed results.

1 Introduction

Continuous interest to coherent population trapping (CPT) and the related electromagnetically induced transparency phenomena is stipulated by a number of important applications in a variety of fields such as laser cooling, information storage, magnetometry, spectroscopy, atomic frequency references etc. [1, 2, 3, 4, 5, 6]. EIT resonance can occur in a Λ -system with two long-lived states and one excited state coupled by two laser fields and displays a strong reduction in absorption where a maximum is expected in the absence of the coupling laser field (EIT can occur also in ladder Ξ - and V -systems). For many applications, it is important to reduce the dimensions of a cell containing atomic metal vapor where

the EIT resonance is formed, at the same time keeping good resonance parameters. The linewidth of the EIT resonance in a Λ -system for the case of low laser intensity is given by $\gamma_{EIT} = 2\Gamma_{21} + \Omega^2/\gamma_N$ [3], where Γ_{21} is the coherence dephasing rate, with Ω being the Rabi frequency and γ_N the natural linewidth. For the case when nanometric-thin cells (NTC) are employed [7, 8, 9, 10], the value of Γ_{21} is highly affected by atom-wall (cell window) collisions; it takes place, though less pronounced, also for sub-millimeter thin cells [11, 12]. It is known that a unique collision with a dielectric surface of an uncoated vapor cell is sufficient to thermalize the ground hyperfine levels, with depolarization probability $0.5 - 1$ (see [13] and references therein). In order to preserve the atomic coherence in wall collisions and to detect ultra-narrow linewidths with the help of coherent processes like EIT, either coated walls or admixture of a buffer gas were used [11]. As the size of a vapor cell is reduced, the lifetime of the ground-state coherence becomes shorter because of collisions of atoms with cell windows: $\Gamma_{21} = (2\pi t)^{-1}$, where $t = L/u$ (L is the distance between windows and u is the most probable thermal velocity). Also the contrast of EIT resonance depends strongly on Γ_{21} . Hence, one could expect that the EIT effect would completely wash out in the case of $L < 1 \mu\text{m}$ ($2\Gamma_{21} > 100$ MHz). Nevertheless, it was demonstrated that the EIT resonance can be observed in thin cells with thickness as small as $\sim 1 \mu\text{m}$ [9, 10]. The explanation for this non-intuitive behavior is as follows: when the coupling laser is resonant with an atomic transition, only the atoms flying nearly parallel to cell windows and hence not experiencing wall collisions do contribute to the formation of the EIT resonance.

In [14] it was shown that for an ordinary cm-size cell, the excitation of the D₁ line results in greater EIT contrast as compared to that for the D₂ line. One of the goals of the present study was to verify whether this statement holds also for the case of NTC by comparing the measured EIT contrast with that observed earlier

Send offprint requests to: A. Papoyan

Correspondence to: papoyan@ipr.sci.am, Institute for Physical Research, NAS of Armenia, Ashtarak-2, 0203, Armenia

for the D_2 line [9,10]. A high contrast is needed, in particular, to detect the splitting of the EIT resonance in an external magnetic field for the thickness as small as $L = \lambda = 794$ nm with a better spectral resolution than that presented in [15]. This may allow one to develop an optical magnetometer with nanometric-range spatial resolution. Switching from D_2 line to D_1 line is also expected to be favorable for forming the EIT resonance both in the absorption and the fluorescence spectra when the cell thickness is $\lambda/2$ (397 nm).

2 Experiment

2.1 Nanometric-thin cell

The design of a NTC is similar to that of extremely thin cell described earlier [7]. The modification implemented in the present work is as follows. The rectangular 20 x 30 mm, 2.5 mm-thick window wafers polished to < 5 nm surface roughness are fabricated from commercial optical grade sapphire (Al_2O_3), which is chemically resistant to hot vapors of alkali metals. The wafers are cut across the c -axis to minimize the birefringence. In order to exploit variable vapor column thickness in the range of 30 - 2000 nm, the cell is vertically wedged by placing a 2 μm -thick platinum spacer strip between the windows at the bottom side prior to gluing. The NTC is filled with a natural rubidium (72.2 % ^{85}Rb and 27.8 % ^{87}Rb). The photograph of the NTC cell is presented in Fig. 1. Since

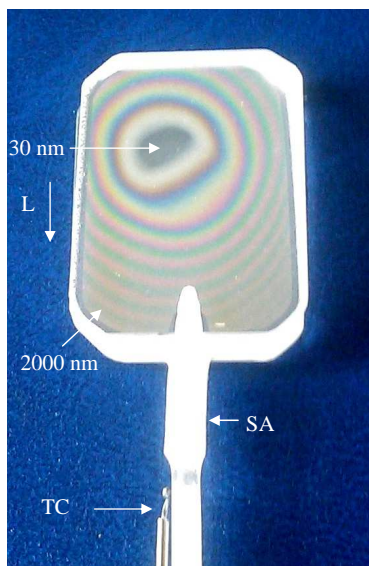


Fig. 1 Photograph of the NTC. The gap thickness L varies from 30 to 2000 nm across the window as visualized by an interference pattern. Regions of $L = 30$ nm and 2000 nm are marked. SA: sapphire side-arm; TC: thermocouple.

the gap between the windows (i.e. the thickness of Rb atomic vapor column) L is of the order of visible light

wavelength, an interference pattern is clearly seen visualizing a smooth thickness variation from 30 nm to 2000 nm. A thermocouple TC is attached to the sapphire side arm (SA) at the boundary of metallic Rb to measure the temperature, which determines the vapor pressure. The SA temperature in present experiment was 120 - 140 $^{\circ}\text{C}$, while the windows temperature was kept some 20 $^{\circ}\text{C}$ higher to prevent condensation. This temperature regime corresponds to atomic number density $N = 1.6 \times 10^{13} - 4.8 \times 10^{13} \text{ cm}^{-3}$. The NTC operated with a special oven with four optical outlets: a pair of in line ports for laser beam transmission and two orthogonal ports to collect the side fluorescence. This geometry allows simultaneous detection of transmission and fluorescence spectra. The oven and NTC assembly was rigidly attached to a translation stage for smooth vertical movement to adjust the needed vapor column thickness without variation of thermal conditions. For more details see [8,16].

2.2 Experimental setup

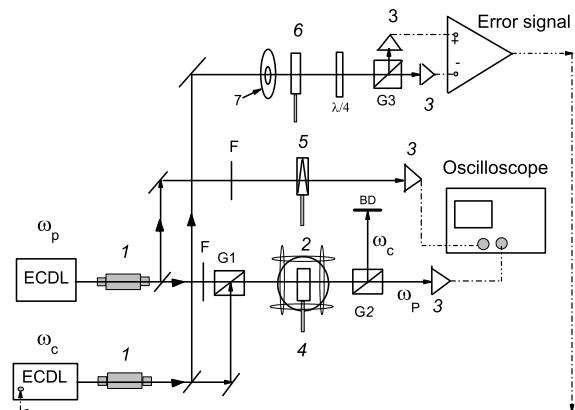


Fig. 2 Sketch of the experimental setup. 1- Faraday isolators; $G_{1,2,3}$ - Glan prisms; 2- Helmholtz coils; 3- photodiodes; 4- main NTC; 5- auxiliary NTC of $L = \lambda$; 6- auxiliary NTC of $L = \lambda/2$; 7- permanent ring magnet (for details, see the text); BD- beam damp.

The experimental arrangement is sketched in Fig. 2. The beams of two separate single-frequency extended cavity diode lasers (ECDL) with $\lambda \approx 794$ nm and ~ 1 MHz linewidth are well superimposed and directed onto the NTC at near-normal incidence by the first Glan prism (G_1). The coupling and probe beams have an elliptical shape of 3×2 mm and have linear and perpendicular polarizations. Faraday isolators (1) are used to prevent an extraneous feedback from reflected beams. Nanometric-thin cell (4) is placed inside the three pairs of mutually perpendicular Helmholtz coils (2) providing the possibility to cancel laboratory magnetic field

as well as to apply homogeneous magnetic field. The transmission and fluorescence radiations are recorded by the photodiodes (β) followed by operation amplifiers; the signal of the photodiodes is recorded by a two-channel digital storage oscilloscope Tektronix TDS 3032B. The radiation power of the coupling and probe lasers was varied throughout the measurement in the range of 1 - 30 mW and 0.01 - 3 mW, respectively using neutral density filters F . An improved Dichroic-Atomic-Vapor-Laser-Locking technique realized with the help of a separate NTC with $L = \lambda/2$, a permanent ring magnet (γ), $\lambda/4$ plate, Glan prism (G_3), and an error signal unit for electronic subtraction of two photodiodes signals is used for the coupling laser frequency stabilization (see [16]). The frequency reference spectrum was formed with the help of an auxiliary NTC (δ) with $L = \lambda$ [16]. A second Glan prism (G_2) was used for separating the coupling and probe beams, so that only the probe beam transmission could be monitored.

2.3 EIT in nanometric-thin cell: the coupling laser is resonant with atomic transition

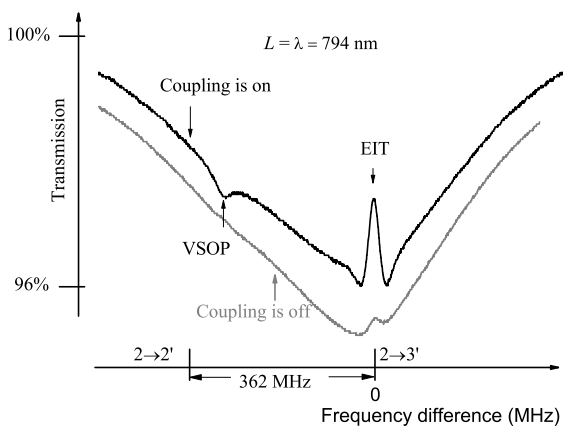


Fig. 3 EIT spectrum for ^{85}Rb D₁ line (upper curve). $L = \lambda = 794$ nm. Coupling laser is resonant with $F = 3 \rightarrow F' = 3$ transition, probe laser is scanned across $F = 2 \rightarrow F' = 2, 3$ transitions. Grey line: the spectrum without the coupling laser (vertically shifted for convenience).

In Fig. 3 is shown the transmission spectrum of the probe laser (the upper curve) for the thickness $L = \lambda$ ($\lambda = 794$ nm) when the 20 mW coupling laser radiation is resonant with $F = 3 \rightarrow F' = 3$ transition, while the 0.04 mW probe laser radiation frequency is scanned across the $F = 2 \rightarrow F' = 2, 3$ transitions (see Fig. 8 in case of zero coupling laser detuning $\Delta = 0$). The full width at half maximum (FWHM) of the EIT resonance is 25 MHz, while the contrast defined as the ratio of the EIT amplitude to the height of the shoulders is 34 %.

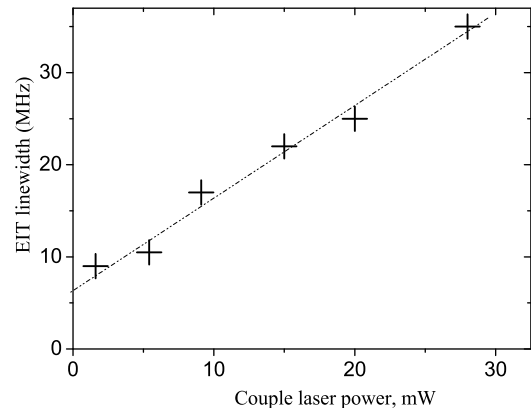


Fig. 4 Dependence of ^{85}Rb D₁ line EIT resonance linewidth on coupling laser power for $\Delta = 0$. $L = \lambda = 794$ nm.

For a higher coupling laser radiation power, 28 mW, the the linewidth broadens to ~ 35 MHz, while the contrast reaches nearly 40 %. Note that the best contrast for D₂ line obtained under similar experimental conditions was 5 - 6 % [9, 10]. The grey line shows the transmission spectrum when the coupling laser is off. The side-arm temperature of NTC is 140 °C (Rb atomic vapor density $N = 4.8 \times 10^{13} \text{ cm}^{-3}$). As is seen, the velocity selective optical pumping (VSOP) peak demonstrates an increase of the absorption, since the coupling laser transfers a number of atoms from $F = 3$ to $F = 2$, thus increasing the probe absorption for $F = 2 \rightarrow F' = 2, 3$ transitions (also the EIT resonance is superimposed on the VSOP at $F = 2 \rightarrow F' = 3$ transition). The theoretical spectrum as obtained from the numerical calculations (see Section 3) is shown in Fig. 7 (the second curve from the bottom, case of $\Delta = 0$) for the same parameters as in Fig. 3 except the probe laser power taken to be 1 mW.

Fig. 4 presents the EIT resonance linewidth as a function of the coupling laser power for $\Delta = 0$. The intersection of the curve with the vertical axis gives the residual coherence dephasing rate of $\gamma'_{21} = 6$ MHz, which is caused by several reasons, including atom-atom, atom-wall collisions in NTC, time-of-flight broadening, as well as due to the fact that the lasers are not coherently coupled [3].

Earlier, it was demonstrated that there is a dramatic difference for the absorption (and also fluorescence) spectrum when the thickness of NTC is reduced from $L = \lambda$ to $L = \lambda/2$, which is caused by the revival of Dicke-type coherent narrowing effect. Particularly, the linewidth of the sub-Doppler absorption spectrum for $L = \lambda/2$ is ~ 3 times narrower than that for $L = \lambda$, while showing the same peak absorption value [18, 19, 20]. Moreover, as it was recently demonstrated, for $L = \lambda/2$ it is impossible to form any type of sub-Doppler dip (VSOP resonance) neither in transmission nor in fluorescence spectra, even

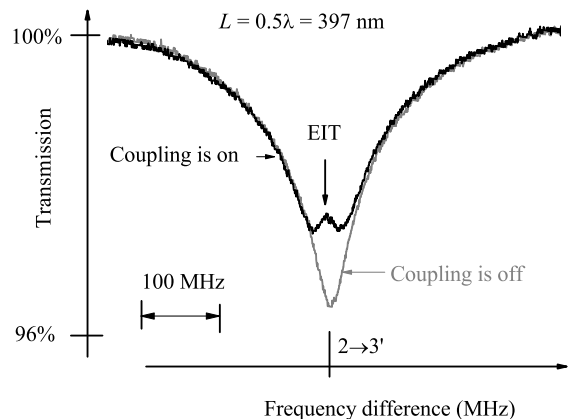
for the laser intensity as high as several tens of W/cm^2 , as opposed to $L = \lambda$ case where only a few mW/cm^2 probe laser intensity is sufficient for a dip formation. For this reason, the $L = \lambda/2$ case is of a particular interest for EIT resonance formation.

The striking point is that it is possible to form an EIT resonance (i.e. a peak of reduced absorption) for the thickness $L = \lambda/2$ already at a coupling laser intensity as low as $\sim 0.1 \text{ W}/\text{cm}^2$ (see Fig. 5(a)). The grey curve shows the 120 MHz-wide sub-Doppler transmission spectrum for $L = \lambda/2$ when the coupling laser is off. The EIT for the thickness $L = \lambda/2$ was theoretically addressed in [10].

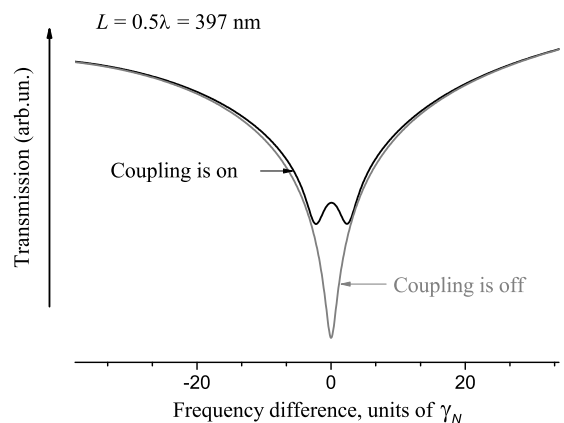
The EIT resonance demonstrating reduction of the fluorescence (dip of reduced fluorescence) for $L = \lambda/2$ is shown in Fig. 6(a). The grey curve shows the sub-Doppler fluorescence spectrum of 70 - 80 MHz linewidth [8] when the coupling laser is off. The theoretical spectra for the parameters matching exactly the corresponding experimental conditions of Figs. 5(a) and 6(a) with $\Omega_c = 1.5\gamma_N$, $\gamma'_{21} = 6 \text{ MHz}$ are shown in Fig. 5(b) (transmission spectrum, $\Omega_p = 0.06\gamma_N$) and Fig. 6(b) (fluorescence spectrum, $\Omega_p = 0.5\gamma_N$). As it is seen, there is a good agreement between the experiment and the theory. Thus, despite the Dicke effect of strong spectrum narrowing and increase of the absorption for $L = \lambda/2$, the increase of coupling laser intensity to $\sim 100 \text{ mW}/\text{cm}^2$ makes it possible to form an EIT resonance both in the absorption and the fluorescence spectra.

2.4 EIT in nanometric-thin cell: dependence on coupling laser detuning

One of the drastic differences in behavior of EIT realized in NTC and in an ordinary 1 - 10 cm long cell is exhibited by the EIT linewidth and amplitude dependence on the coupling laser detuning Δ (see Fig. 8). The EIT linewidth and amplitude (contrast) as a function of blue detuning Δ of the coupling laser for $L = \lambda$ can be evaluated from the experimental and theoretical transmission spectra shown in Fig. 7. The side-arm temperature of NTC is $140 \text{ }^\circ\text{C}$, $P_c \approx 20 \text{ mW}$. In order to get more prominent EIT resonance for the large values of detuning, the probe laser radiation power was increased to 1 mW . As it is seen, the increase of detuning Δ from 0 to 40 and 85 MHz results in rapid broadening of EIT resonance linewidth from 25 MHz to 50 and 80 MHz FWHM, correspondingly, meanwhile the EIT amplitude rapidly decreases. This behavior has the following physical explanation. For the case of an exact atomic resonance ($\Delta = 0$), mainly the atoms flying parallel to NTC windows contribute to formation of the EIT resonance. The interaction time for these atoms is $\tau_D = D/v$, where D is the laser beam diameter ($D \gg L$). When the coupling laser is detuned from an atomic transition by a value of Δ , only those atoms having the ve-



(a)



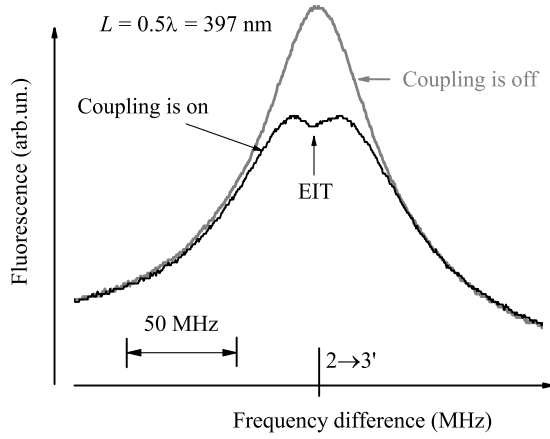
(b)

Fig. 5 Probe laser transmission spectrum for ^{85}Rb D_1 line. $L = \lambda/2 = 397 \text{ nm}$. Coupling laser ($P_c = 27 \text{ mW}$) is resonant with $F = 3 \rightarrow F' = 3$ transition, probe laser ($P_p = 0.04 \text{ mW}$) is scanned across $F = 2 \rightarrow F' = 2, 3$. Grey line: spectrum when coupling laser is off. Graph *a*: experiment; graph *b*: numerical calculations for the experimental parameters, $\Omega_c = 1.5\gamma_N$, $\Omega_p = 0.06\gamma_N$, $\gamma'_{21} = 6 \text{ MHz}$.

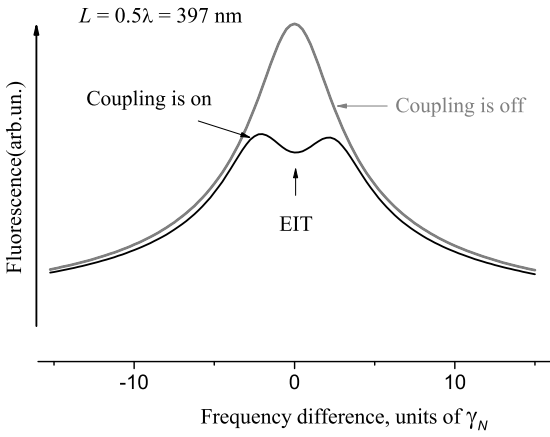
locity projection $v_z = 2\pi\Delta/k$ contribute to the formation of EIT, and for these atoms the flight time between the cell windows shortens with the detuning increase: $\tau_L = L/v_z = kL/(2\pi\Delta)$. This causes frequent quenching collisions of atoms with the cell windows leading to the increase of γ'_{21} and consequently, to strong linewidth broadening and contrast reduction of the EIT resonance. For this case γ_{EIT} can be described by a simple expression

$$\gamma_{EIT}(\Delta) = \gamma_{EIT}|_{\Delta=0} + 2\gamma'_{21}(\Delta), \quad (1)$$

where $\gamma'_{21}(\Delta) = 1/(2\pi\tau_L)$. Replacing the gap thickness by a justified parameter $L_{eff} = L/2$, we get $\gamma'_{21}(\Delta) = \Delta/\pi$ for $L = \lambda$. From (1) for $\Delta = 40$ and 85 MHz we have $\gamma_{EIT} = 50$ and 79 MHz , correspondingly, which is in



(a)



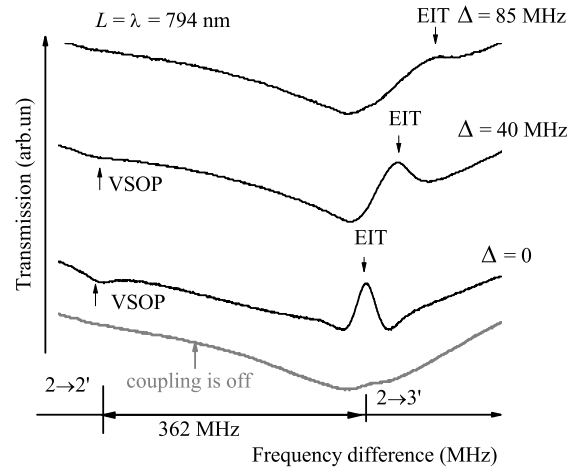
(b)

Fig. 6 Transmission spectrum of the probe laser for ^{85}Rb D₁ line, $L = \lambda/2 = 397$ nm. Coupling laser ($P_c = 27$ mW) is resonant with $F = 3 \rightarrow F' = 3$ transition, probe laser ($P_p = 3$ mW) is scanned across $F = 2 \rightarrow F' = 2, 3$. Grey line: the coupling laser is off. Graph *a*: experiment; graph *b*: numerical calculations for the experimental parameters, $\Omega_c = 1.5\gamma_N$, $\Omega_p = 0.5\gamma_N$, $\gamma'_{21} = 6$ MHz.

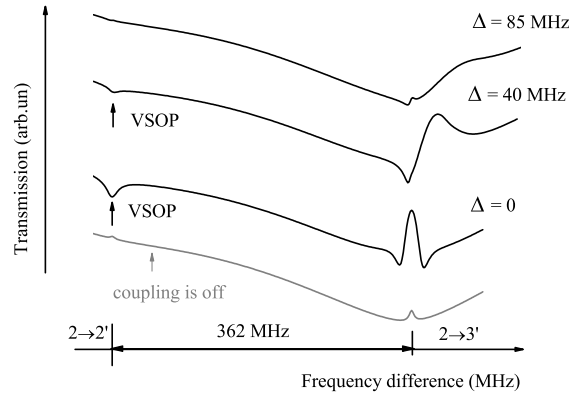
good agreement with the experimental values. We should note that measurement of EIT resonance linewidth γ_{EIT} at large coupling laser detuning could serve as a convenient tool to study atom-window collisions and properties of window material.

This behavior completely differs from that observable in ordinary 1 - 10 cm long cell where formation of EIT resonance on the wings of the Doppler profile of the absorption line can lead to its narrowing [21] as opposed to the case of NTC.

It is well known that addition of a buffer gas into 1 - 10 cm long ordinary cell improves EIT resonance parameters [3, 4]. The preliminary results have shown that



(a)



(b)

Fig. 7 EIT spectra for $L = \lambda = 794$ nm when the coupling laser is detuned by Δ from $F = 3 \rightarrow F' = 3$ transition. The spectra are shifted vertically for convenience. The lower grey curve is the transmission spectrum when the coupling laser is off. Graph *a*: experiment; graph *b*: numerical calculations for the experimental conditions, $\Omega_c = 1.3\gamma_N$, $\Omega_p = 0.3\gamma_N$, $\gamma'_{21} = 6$ MHz. Additional dephasing rate $\gamma'_{21}(\Delta)$ is responsible for the EIT behavior seen for $\Delta \neq 0$ (see the text).

admixture of 20 Torr of N₂ buffer gas to Rb vapor in NTC leads to decrease of EIT broadening rate with the increase of Δ . This is explained by substantial shortening of the mean free path of Rb atoms due to Rb-N₂ collisions (~ 300 nm), which becomes less than the NTC thickness ($L = 794$ nm). However, at $\Delta = 0$ there appears undesirable supplementary broadening: Rb atoms flying parallel to the NTC windows experience velocity changing collisions with N₂, change their direction and collide with the windows, which leads to the increase of Γ_{21} .

2.5 Splitting of EIT resonance in magnetic field, $L = \lambda$

In [9] it was shown that using NTC with Rb vapor of $L = 2\lambda$ thickness ($\lambda = 780$ nm), one can measure a magnetic field by splitting EIT resonances formed at D_2 line excitation. However, due to a small contrast of the EIT resonance it was impossible to detect the splitting at smaller L values. Switching to D_1 excitation allowed us to improve the EIT contrast and thus to detect the splitting for $L = \lambda = 794$ nm as is shown in Fig. 9. The measurement shown in the upper curve was done with application of $B = 14$ G longitudinal magnetic field ($\mathbf{B} \parallel \mathbf{k}$), for laser radiation powers $P_c = 5$ mW and $P_p = 0.05$ mW. Three well resolved EIT resonances are clearly seen in the upper curve; the lower curve presents the EIT resonance when $B = 0$. In [9] it was shown that in this case three A -systems are formed, and the frequency separation between these EIT components is $1.4 \text{ MHz/G} \times 14 \text{ G} = 19.6 \text{ MHz}$. The inset presents the results of fitting by Gaussian function resulting in the linewidth of 10 MHz FWHM for an individual EIT component. Note that the exact splitting value for strong B fields is given by the Rabi-Breit formula [3].

So-called " λ -Zeeman technique" (LZT) to investigate atomic transitions in magnetic field was presented in [15]. Rb atoms are confined in a NTC with $L = \lambda$. Narrow VSOP resonances of 30 - 35 MHz linewidth formed in a single beam in transmission spectrum are split into several components in a magnetic field; their frequency positions and transition probabilities depend on the B field. As one can see in Fig. 9, the observed splitting of EIT resonance provides a spectral resolution, which is better than that for LZT by a factor of 3 [15]. Moreover, among the inherent advantages of NTC is the possibility to apply very high magnetic field using widely available strong permanent ring magnets (our Helmholtz coils produce $B < 200$ G). In spite of a strong inhomogeneity of the B field (it can reach ~ 150 G/mm in axial direction), the variation of B inside the atomic vapor column does not exceed ~ 0.1 G (several orders less than the applied B value) because of sub-micrometer thickness of the NTC. Our preliminary results show that it is realistic and straightforward to determine a spatially-localized value of a B field in the range of 1 - 1000 G with nearly the same precision throughout the whole range, by measuring the frequency interval between the EIT components. This is especially valuable for mapping of strongly non-homogeneous magnetic field.

3 Theoretical model

To calculate the observed EIT resonances we consider four-level A -type atomic systems consisting of two ground hyperfine levels ($F_g = 2, 3$) and two excited levels ($F_e = 2, 3$) in the D_1 line of ^{85}Rb (see Fig. 8) confined in a cell of thickness L . The probe field E_p (with center angular

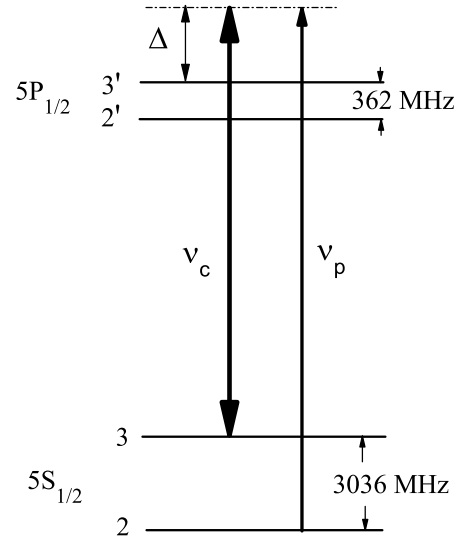


Fig. 8 Relevant energy levels of ^{85}Rb D_1 line involved in EIT process. The coupling laser detuning Δ varies from $F = 3 \rightarrow F' = 3$ transition in the range of 0 - 100 MHz.

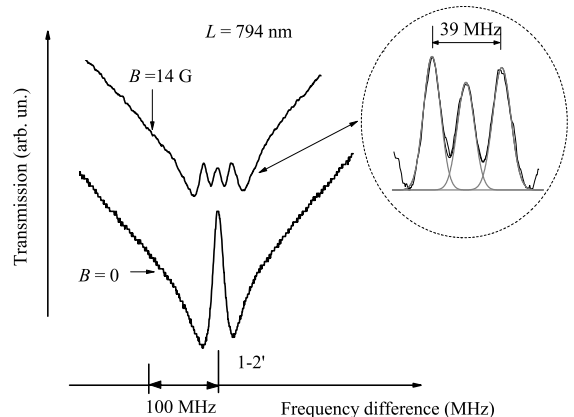


Fig. 9 Probe laser transmission spectrum for $L = \lambda = 794$ nm with a longitudinal magnetic field $B = 14$ G (upper curve). $P_c = 5$ mW, $P_p = 0.05$ mW. Splitting of EIT resonance to three components is well seen. The inset shows the results of fitting by a Gaussian function (grey lines); FWHM of an individual EIT component is 10 MHz. Lower curve: the EIT resonance for $B = 0$.

frequency ω_p) and the coupling field E_c (with angular frequency ω_c) couple the transitions $|1\rangle \rightarrow |3\rangle, |4\rangle$ and $|2\rangle \rightarrow |3\rangle, |4\rangle$, respectively (see Fig. 10). For simplicity, we restrict ourselves to one dimensional situation where the two driving linearly polarized laser radiations are in the $\pm z$ -direction. The probe and coupling lasers are detuned from the corresponding atomic resonances by

$$\begin{aligned} \Delta_{p1,p2} &= \omega_p - \omega_{3,4;1} - k_p v_z, \\ \Delta_{c1,c2} &= \omega_c - \omega_{3,4;2} - k_c v_z, \end{aligned} \quad (2)$$

where the subscripts $p(c)$ mark the detunings for the probe (coupling) lasers, ω_{ij} is the frequency difference between levels i and j , and $k_{p,c}v_z$ are the Doppler shifts for atoms corresponding to the velocity component v_z along the propagation vectors $\mathbf{k}_{p,c}$. The total Hamiltonian of the system is given by $\hat{H} = \hat{H}_0 + \hat{H}_I$, where \hat{H}_0 describes a free atom and \hat{H}_I describes the interaction between the atom and the electric fields. With electric-dipole and rotating-wave approximations, the interaction Hamiltonian \hat{H}_I of the system is given by

$$\hat{H}_I = -\hbar(\Omega_{p1}|3\rangle\langle 1| + \Omega_{p2}|4\rangle\langle 1| + \Omega_{c1}|3\rangle\langle 2| + \Omega_{c2}|4\rangle\langle 2|) + \text{H.c.}, \quad (3)$$

where $\Omega_{p1,p2} = \mu_{1,3,4}E_p/2\hbar$ and $\Omega_{c1,c2} = \mu_{2,3,4}E_c/2\hbar$ are the Rabi frequencies of the probe and coupling fields, respectively, with μ_{ij} being the electric-dipole matrix element associated with the transition from j to i , and H.c. represents Hermitian conjugate. To describe the dynam-

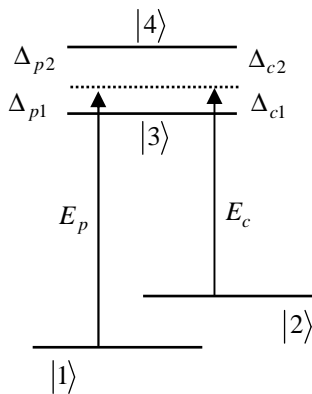


Fig. 10 A-type four-level atomic system.

ics of the system driven by this Hamiltonian we adopt here the theoretical model presented in Ref. [10]. Interested readers may refer to this work and to the references therein for the mathematical details of the calculations. We summarize here the main features of the approach used. The basic assumptions made in the model are as follows: the atomic number density is assumed to be low enough so that the effect of collisions between the atoms can be ignored; the atoms experience inelastic collisions with the cell walls; the incident beam diameters largely exceed the cell thickness. The internal atomic dynamics is described by a semiclassical density matrix $\rho = \sum \rho_{ij}|i\rangle\langle j|$, the time evolution of which is given by the Liouville equation of motion :

$$\dot{\rho} = -i/\hbar[\hat{H}, \rho] + \Gamma\rho, \quad (4)$$

where Γ is the relaxation operator : $\Gamma_{ij} = \frac{1}{2}(\gamma_i + \gamma_j) + \gamma_{ij}\delta_{ij}$. Here γ_i , γ_j are the natural decay rates of states $|i\rangle$ and $|j\rangle$, and γ_{ij} is the pure dephasing rate.

To obtain the probe transmission spectra, we provide an exact numerical solution of the set of optical

Bloch equations deduced from Eq. (4) and coupled to Maxwell equations [22]. In accordance with the assumptions made, we neglect the collisional broadening of optical transitions compared to the spontaneous decay rate, the relaxation of atoms traveling out of the diameter of the laser beam. The dephasing rate of the ground-state coherence, Γ_{21} , is determined in the model by the finite time of flight of atoms between the cell windows. This parameter, usually introduced into theoretical calculations as a phenomenological constant to fit the experimental data, is taken into account in the model exactly by solving the temporal density-matrix equations with proper boundary conditions for each atom separately.

A number of relevant parameters, both inherent to the atomic system and the experimental setup, are included into the model such as Doppler broadening, phase fluctuations in the laser fields [23,24], non-correlation of the laser fields [3]. The light reflections on the locally highly-parallel cell walls of a nano-cell behaving as a Fabry-Pérot cavity [25] is taken into account. For the Rabi frequency the estimates are obtained from $\Omega/2\pi = a\gamma(I/8)^{1/2}$, where I is the laser intensity in mW/cm², γ is the decay rate of the excited state, and a is a fit parameter (for our case $a \approx 0.2$) [27]. A general agreement between the results of our calculations and that of the experiment is seen.

4 Discussion

Miniaturization of EIT setup without loss of resonance characteristics is among the challenges for technological implementation of the electromagnetically induced transparency. The results obtained in the present study are not intuitive, and it is worth to compare them with the relevant results presented in literature, and analysing the distinctions. In [26] a similar setup was employed for the EIT studies: two separate lasers of 1 MHz linewidth and approximately the same power were used to form the EIT resonance on D₁ line of Rb. The vapor was confined in a 3 cm-long glass cell. The following key parameters have been achieved: $\sim 60\%$ for the EIT resonance contrast, and ~ 20 MHz for the spectral width. The corresponding values obtained in the present work with the use of $L = 794$ nm NTC are $\sim 40\%$ and ~ 35 MHz, respectively. Thus, decreasing the cell length by a factor of 3.8×10^4 does not lead to a dramatic deterioration of the key parameters of EIT.

Sub-millimeter-thick cells have been used in [11,12] for EIT formation. In recent works [28,29] EIT resonance is formed in Rb vapor generated in hollow-core photonic band-gap (HCPBG) of inner diameter 6 μ m and $L = 25$ cm. Large L together with high laser intensity achieved in HCPBG leads to the decrease of threshold laser power for EIT formation. However, the width of EIT resonance reaches ~ 100 MHz, which exceeds by an order of magnitude the width of EIT resonance in NTC. Moreover,

the realization of HCPBG method is rather complicated technically.

There are yet other papers where suggestions to improve the EIT characteristics in thin cells are addressed. In [30] formation of narrow EIT resonance in nano-cells is proposed by using supplementary anti-relaxation coating for windows, aiming at decrease of coherence dephasing rate. However, the realisation of such a coating is not yet feasible. Formation of regions of few tens of micrometer in quartz substrate-window is realized using chemical etching with subsequent filling these regions with Rb vapor [17], meanwhile the realization of EIT in such a structure has not been yet discussed. Based on the above analysis, we believe the most convenient and technically justified option for obtaining narrow-linewidth and high-contrast EIT resonances is the NTC scheme presented in this work (note that the NTC has been successfully used also for EIT registration in a ladder Ξ -system [31]).

As it follows from the obtained results, the decrease of L is compensated by an increase of Rb atomic density, so that the product $N \times L$ practically does not change. An important particularity of EIT is the weak influence of $5P_{1/2}$ level broadening on the EIT parameters (in contrast, $5P_{1/2}$ level broadening dramatically affects the amplitude of the VSOP resonance). The latter can allow one to form EIT resonance for $L < 100$ nm by increasing the density N and improving the laser parameters (for example, by the technique of phase-locking the coupling and probe lasers [32]), realization of lock-in detection, etc. Such a small thickness of the NTC is of interest for the study of van der Waals interaction of atoms with dielectric windows [33].

5 Conclusion

The peculiarities of the EIT phenomenon are studied in transmission and fluorescence spectra under D_1 line excitation of rubidium atoms with the help of nanometric-thin vapor cell with a possibility to exploit vapor column thickness L in the range of 400 - 800 nm. The striking point of the present work is that the reduction of L by more than 4 orders as compared with an ordinary cm-size cell does not worsen the high contrast of EIT peak (up to 40 %). This relatively weak thickness dependence is explained by involvement of atoms with particular velocity components in EIT resonance formation: when the coupling laser is resonant with the atomic transition only the atoms moving parallelly to the NTC windows contribute to the EIT formation, and the quenching collisions with the windows are not essential. The situation is dramatically different when the coupling laser is detuned from the atomic transition. In this case the atoms having velocity component towards the windows are responsible for the EIT, they experience collisions with the windows resulting in broadening and contrast worsening of the resonance. It is justified that with the help of the

NTC with $L = \lambda$ and for a large frequency detuning Δ of the coupling laser from atomic resonance it is possible to directly reveal and evaluate the strong influence of atom-walls collisions on the EIT linewidth. By changing the value of Δ one can smoothly control the EIT linewidth and contrast; measurement of the EIT linewidth makes it possible to determine the atom-wall collision rate. The theoretical model well describes the observed results. Formation of the EIT resonance in a Λ -system for even smaller thickness (below 100 nm) can offer a possibility for quantitative study of atom-surface van der Waals interaction.

For the first time, it is demonstrated that despite the Dicke-effect of strong spectrum narrowing and increase of the absorption when thickness is $L = \lambda/2$ (397 nm), the relatively low intensity of the coupling laser is sufficient to form the EIT resonance both in the absorption and the fluorescence spectra. This is the minimal L for the coherent process reported so far.

It is shown that the EIT resonance in a NTC with $L = \lambda$ splits in an external magnetic field to well-resolved components that may allow one to develop magnetometer with nanometric-range spatial resolution. This can be of importance for measuring and mapping the strongly non-homogeneous magnetic field.

6 Acknowledgement

The authors are grateful to A. Sarkisyan for his valuable participation in fabrication of the NTC and to Charles Adams for useful discussions. Research conducted in the scope of the International Associated Laboratory IR-MAS. Armenian team thanks for the ANSEF Opt-2428 support. R. M. acknowledges the support from the NF-SAT, NAS RA and CRDF (grant no. ECSP-10-10 GRSP).

References

1. G. Alzetta, A. Gozzini, L. Moi, and G. Orriols, *Nuovo Cimento Soc. Ital. Fis. B*, **36**, 5 (1976).
2. E. Arimondo, *Progress in Optics*, Elsevier, Amsterdam 1996.
3. R. Wynands, A. Nagel, *Appl. Phys. B, Lasers Opt.* **68**, 1 (1999).
4. M. Fleischhauer, A. Imamoglu, and J. P. Marangos, *Rev. Mod. Phys.* **77**, 633 (2005).
5. J. Vanier, *Appl. Phys. B*, **81**, 421 (2005).
6. A. K. Mohapatra, T. R. Jackson, C. S. Adams, *Phys. Rev. Lett.* **98**, 113003 (2007).
7. D. Sarkisyan, D. Bloch, A. Papoyan, M. Ducloy, *Opt. Commun.* **200**, 201 (2001).
8. D. Sarkisyan, T. Becker, A. Papoyan, P. Thoumany, H. Walther, *Appl. Phys. B* **76**, 625 (2003).
9. A. Sargsyan, D. Sarkisyan, A. Papoyan, *Phys. Rev. A* **73**, 033803 (2006).
10. Y. Pashayan-Leroy, C. Leroy, A. Sargsyan, A. Papoyan, D. Sarkisyan, *J. Opt. Soc. Am. B* **24**, 1829 (2007).

11. S. Knappe, L. Hollberg, J. Kitching, *Opt. Lett.* **29**, 388 (2004).
12. K. Fukuda, A. Toriyama, A. Izmailov, M. Tachikawa, *Appl. Phys. B*, **80**, 503 (2005).
13. H.N. De Freitas, M. Oria, M. Chevrollier, *Appl. Phys. B* **75**, 703 (2002).
14. M. Stähler, R. Wynands, S. Knappe, J. Kitching, L. Hollberg, A. Taichenachev, V. Yudin, *Optics Lett.* **27**, 1472 (2002).
15. A. Sargsyan, G. Hakhumyan, A. Papoyan, D. Sarkisyan, A. Atvars, M. Auzinsh, *Appl. Phys. Lett.* **93**, 021119 (2008).
16. A. Sargsyan, A.V. Papoyan, D. Sarkisyan, A. Weis, *Eur. Phys. J.- Appl. Phys.* **48**, 20701 (2009).
17. T. Baluktian, C. Urban, T. Bublat, H. Giessen, R. Löw, T. Pfau, *Optics Lett.* **35**, 1950 (2010).
18. G. Dutier, A. Yarovitski, S. Saltiel, A. Papoyan, D. Sarkisyan, D. Bloch, M. Ducloy, *Europhys. Lett.* **63**, 35 (2003).
19. D. Sarkisyan, T. Varzhapetyan, A. Sarkisyan, Yu. Malakyan, A. Papoyan, A. Lezama, D. Bloch, M. Ducloy, *Phys. Rev. A* **69**, 065802 (2004).
20. C. Andreeva, S. Cartaleva, L. Petrov, S. M. Saltiel, D. Sarkisyan, T. Varzhapetyan, D. Bloch, M. Ducloy, *Phys. Rev. A* **76**, 013837 (2007).
21. J. Wang, Y. Wang, S. Yan, T. Liu, T. Zhang, *Appl. Phys. B*, **78**, 217 (2004).
22. B. W. Shore, *The Theory of Coherent Atomic Excitation*, John Wiley & Sons, New York 1990.
23. G. S. Agarwal, *Phys. Rev. Lett.* **37**, 383 (1976).
24. B. J. Dalton and P. L. Knight, *Opt. Commun.* **42**, 411 (1982).
25. G. Dutier, S. Saltiel, D. Bloch and M. Ducloy, *J. Opt. Soc. Am. B*, **20**, 793 (2003).
26. X. Wei, J. Wu, G. Sun, Z. Shao, Z. Kang, Y. Jiang, J-Y.Gao, *Phys. Rev. A* **72**, 023806 (2005).
27. A. J. Krmpot, M. M. Mijailovic, B. M. Panic, D. V. Lukic, A. G. Kovacevic, D. V. Pantelic, B. M. Jelenkovic, *Opt. Express* **13**, 1448 (2005).
28. S. Ghosh, A. R. Bhagwat, C. K. Renshaw, S. Goh, A. L. Gaeta, B. J. Kirby, *Phys. Rev. Lett.* **97**, 023603 (2006).
29. A. D. Slepko, A. R. Bhagwat, V. Venkataraman, P. Londero, A. L. Gaeta, *Phys. Rev. A*, **81**, 053825 (2010).
30. A.N. Litvinov, G.A. Kazakov, B.G. Matisov, *J. Phys. B, At. Mol. Opt. Phys.* **42**, 165402 (2009).
31. A. Sargsyan, D. Sarkisyan, U. Krohn, J. Keaveney, Ch. Adams, *Phys. Rev. A*, **82**, 045806 (2010).
32. D. Höckel, M. Scholz, O. Benson, *Appl. Phys. B*, **94**, 429 (2009).
33. M. Fichet, G. Dutier, A. Yarovitsky, P. Todorov, I. Hamdi, S. Saltiel, D. Sarkisyan, M-P. Gorza, D. Bloch, M. Ducloy, *Europhys. Lett.* **77**, 54001 (2007).